









# Modeling Phenotypic Heterogeneity of Glycogen Storage Disease Type 1a Liver Disease in Mice by Somatic CRISPR/CRISPR-associated protein 9–Mediated Gene Editing

Martijn G.S. Rutten <sup>1</sup>, Terry G.J. Derks <sup>2</sup>, Nicolette C.A. Huijkman,<sup>1</sup> Trijnie Bos,<sup>3</sup> Niels J. Kloosterhuis,<sup>1</sup> Kees C.W.A. van de Kolk,<sup>4</sup> Justina C. Wolters <sup>1</sup>, Mirjam H. Koster <sup>1</sup>, Laura Bongiovanni <sup>5</sup>, Rachel E. Thomas,<sup>5</sup> Alain de Bruin <sup>1,5</sup>, Bart van de Sluis <sup>1</sup>, and Maaïke H. Oosterveer <sup>1</sup>

**BACKGROUND AND AIMS:** Patients with glycogen storage disease type 1a (GSD-1a) primarily present with life-threatening hypoglycemia and display severe liver disease characterized by hepatomegaly. Despite strict dietary management, long-term complications still occur, such as liver tumor development. Variations in residual glucose-6-phosphatase (G6PC1) activity likely contribute to phenotypic heterogeneity in biochemical symptoms and complications between patients. However, lack of insight into the relationship between G6PC1 activity and symptoms/complications and poor understanding of the underlying disease mechanisms pose major challenges to provide optimal health care and quality of life for GSD-1a patients. Currently available GSD-1a animal models are not suitable to systematically investigate the relationship between hepatic G6PC activity and phenotypic heterogeneity or the contribution of gene-gene interactions (GGIs) in the liver.

**APPROACH AND RESULTS:** To meet these needs, we generated and characterized a hepatocyte-specific GSD-1a mouse model using somatic CRISPR/CRISPR-associated protein 9 (Cas9)–mediated gene editing. Hepatic *G6pc* editing reduced hepatic G6PC activity up to 98% and resulted

in failure to thrive, fasting hypoglycemia, hypertriglyceridemia, hepatomegaly, hepatic steatosis (HS), and increased liver tumor incidence. This approach was furthermore successful in simultaneously modulating hepatic G6PC and carbohydrate response element-binding protein, a transcription factor that is activated in GSD-1a and protects against HS under these conditions. Importantly, it also allowed for the modeling of a spectrum of GSD-1a phenotypes in terms of hepatic G6PC activity, fasting hypoglycemia, hypertriglyceridemia, hepatomegaly and HS.

**CONCLUSIONS:** In conclusion, we show that somatic CRISPR/Cas9-mediated gene editing allows for the modeling of a spectrum of hepatocyte-borne GSD-1a disease symptoms in mice and to efficiently study GGIs in the liver. This approach opens perspectives for translational research and will likely contribute to personalized treatments for GSD-1a and other genetic liver diseases. (HEPATOLOGY 2021;74:2491–2507).

**G**lycogen storage disease type 1a (GSD-1a; MIM#232200) is a rare inborn error of metabolism caused by mutations in the

*Abbreviations:* AFP, alpha-fetoprotein; Cas9, CRISPR-associated protein 9; ChREBP $\alpha/\beta$ , carbohydrate response element-binding protein alpha/beta; CK19, cytokeratin 19; EV, empty vector; FFAs, free fatty acids; G6P, glucose-6-phosphate; G6PC/G6Pase- $\alpha$ , glucose-6-phosphatase, catalytic subunit; GGIs, gene-gene interactions; GPC3, glypican-3; GSD-1a, glycogen storage disease type 1a; GYS2, glycogen synthase 2; H&E, hematoxylin and eosin; HB, hepatoblastoma; HCA, hepatocellular adenoma; HCC, hepatocellular carcinoma; Heppar1, hepatocyte paraffin 1; HS, hepatic steatosis; IQR, interquartile range; ORO, Oil Red O; PAS, periodic acid Schiff; PYGL, glycogen phosphorylase L; sgChrebpa, sgRNAs targeting exon 1 of Chrebpa; sgG6pc, sgRNAs against exon 1 of G6pc; sgRNA, single-guide RNA; TG, triglyceride; UGP2, UDP-glucose pyrophosphorylase 2; vp, viral particles.

Received September 29, 2020; accepted June 9, 2021.

Additional Supporting Information may be found at [onlinelibrary.wiley.com/doi/10.1002/hep.32022/supinfo](https://onlinelibrary.wiley.com/doi/10.1002/hep.32022/supinfo).

Supported by a VIDI grant (91717373) from the Dutch Scientific Organization and by the UMCG Cancer Research Foundation. M.H.O holds a Rosalind Franklin Fellowship from the University of Groningen.

© 2021 The Authors. HEPATOLOGY published by Wiley Periodicals LLC on behalf of American Association for the Study of Liver Diseases. This is an open access article under the terms of the Creative Commons Attribution-NonCommercial-NoDerivs License, which permits use and distribution in any medium, provided the original work is properly cited, the use is non-commercial and no modifications or adaptations are made.

View this article online at [wileyonlinelibrary.com](https://onlinelibrary.wiley.com).

glucose-6-phosphatase (*G6PC1*; G6Pase- $\alpha$ ) gene.<sup>(1)</sup> *G6PC1* (*G6pc* in mice) encodes the enzyme that converts glucose-6-phosphate (G6P) into glucose in hepatocytes, kidney cells, and enterocytes. GSD-1a is biochemically characterized by (fasting) hypoglycemia, hyperlipidemia, hyperlactatemia, and hyperuricemia,<sup>(2)</sup> which are largely attributed to hepatocyte-specific impairment of G6PC activity.<sup>(3)</sup> In addition, patients display a severe hepatic phenotype, characterized by hepatomegaly attributable to the accumulation of glycogen and lipids. After the introduction of dietary management by continuous gastric drip feeding and subsequently uncooked cornstarch in the 1970s/1980s, mortality has been drastically reduced.

Development of liver tumors represents a major long-term complication in GSD-1a patients that is hepatocyte-borne,<sup>(3)</sup> starts to emerge mostly in the second decade of life, and affects 60%-70% of all patients by the age of 30 years.<sup>(4)</sup> The molecular mechanisms underlying the initiation and progression of liver tumors in GSD-1a remain largely unresolved. Poor metabolic control, marked by persistent and severe hypertriglyceridemia,<sup>(4-6)</sup> is associated with an increased risk for liver tumor development in GSD-1a patients.<sup>(7-10)</sup> Importantly, we and others have reported considerable variability in plasma triglyceride (TG) levels between individual GSD-1a patients.<sup>(7,11)</sup> This phenotypic heterogeneity is incompletely understood, but presumably related to a combination of genetic and environmental factors.<sup>(11)</sup> Thus, the current lack of complete insight into the origin of the phenotypic

heterogeneity in symptoms and complications, as well as the mechanisms of liver tumor formation, pose major challenges to optimal health care for GSD-1a patients. This was recently highlighted in the top research priorities identified by the international liver GSD priority setting partnership.<sup>(12)</sup>

Recent studies by our lab and others have identified different intracellular pathways that contribute to GSD-1a liver disease pathophysiology,<sup>(13-21)</sup> or that may compensate for the primary defect in G6PC activity, such as alpha-glucosidase-dependent glycogen breakdown.<sup>(22)</sup> As a result, there is a growing interest to systematically investigate the contribution of specific genes to GSD-1a symptoms and complications in preclinical *in vivo* models. However, when using classical knockout animal models, simultaneous editing of multiple genes is typically time-, resource-, and labor-intensive and requires considerable animal use. In addition, most mouse models are homozygous for the knockout allele with complete deficiency of hepatic G6PC activity,<sup>(23-25)</sup> which hampers the possibility of modeling variations in residual enzyme activities that are typically observed in GSD-1a patients.<sup>(2,6,26)</sup> This limits the translational value of such models with regard to the phenotypic heterogeneity observed in GSD-1a patients.

In order to obtain such insights, it is critical to model residual G6PC activity and elucidate the contribution of gene-gene interactions (GGIs) to symptoms, complications, and interventions.<sup>(12)</sup> Previously, our laboratory successfully applied somatic CRISPR/CRISPR-associated protein 9 (Cas9)-mediated

DOI 10.1002/hep.32022

Potential conflict of interest: Nothing to report.

## ARTICLE INFORMATION:

From the <sup>1</sup>Department of Pediatrics, University Medical Center Groningen, University of Groningen, Groningen, The Netherlands; <sup>2</sup>Section of Metabolic Diseases, Beatrix Children's Hospital, University Medical Center Groningen, Groningen, The Netherlands; <sup>3</sup>Department of Laboratory Medicine, University Medical Center Groningen, University of Groningen, Groningen, The Netherlands; <sup>4</sup>Central Animal Facility, Groningen Small Animal Imaging Facility (Gronsai), University Medical Center Groningen, University of Groningen, Groningen, The Netherlands; <sup>5</sup>Dutch Molecular Pathology Center, Faculty of Veterinary Medicine, Utrecht University, CL Utrecht, The Netherlands.

## ADDRESS CORRESPONDENCE AND REPRINT REQUESTS TO:

Maaïke H. Oosterveer, Ph.D.  
Department of Pediatrics, University Medical Center Groningen  
Internal Zip Code CA84  
Room Y2.147

Hanzeplein 1  
9713 GZ Groningen, The Netherlands  
E-mail: m.h.oosterveer@umcg.nl  
Tel.: +31 (0)50 361 1253

gene editing to systemically investigate the functions of hepatic genes at any desired stage of postnatal life.<sup>(27,28)</sup> In the current study, we applied this gene editing technology to generate a cohort of mice that displays the heterogeneity of hepatic GSD-1a, which can be used as a preclinical “reference population.” As a proof of concept for simultaneous multiple gene editing, we simultaneously deleted hepatocytic *G6pc* and carbohydrate response element-binding protein alpha (*Chrebpa*). Our results illustrate that somatic CRISPR/Cas9-mediated gene editing provides a versatile preclinical platform to rapidly assess the contribution of GGIs to GSD-1a pathophysiology and investigate the relationship between residual enzyme activity and disease pathophysiology.

## Materials and Methods

### ANIMAL EXPERIMENTATION

Male adult (9–14 weeks) hepatocyte-specific, Cas9-expressing mice (obtained by crossing Rosa26-LSL-Cas9 knock-in mice [#024857; The Jackson Laboratory, Bar Harbor, ME] with Alb-cre mice<sup>(27)</sup>) were individually housed in individually ventilated cages with wood bedding, nesting material, and cardboard rolls in a light- and temperature-controlled facility (12-hour light/12-hour dark cycle lighting regime) and fed a standard laboratory chow diet *ad libitum* (RM1; Special Diet Services, Essex, UK). All experimental procedures were approved by the Institutional Animal Care and Use Committee of the University of Groningen (Groningen, The Netherlands) and are in line with the Guide for the Care and Use of Laboratory Animals. For the *G6pc*-targeting experiments, mice received three single-guide RNAs (sgRNAs) against exon 1 of *G6pc* (sg*G6pc*), using an adenoviral gene delivery system ( $0.1$ – $1.0 \times 10^{11}$  viral particles [vp] per mouse) or the pX459 vector (Addgene plasmid #48139; Addgene, Watertown, MA) without any sgRNAs as an empty vector control virus (EV; “control animals”) by intravenous injection in  $100 \mu\text{L}$  of sterile PBS into the retro-orbital plexus under isoflurane anesthesia. The total number of adenoviral particles was adjusted to  $1.0 \times 10^{11}$  per animal using EV, unless stated otherwise. Fed blood glucose levels were measured 2 weeks after virus injection, and fasting blood glucose levels were measured after

overday fasting (8:00 AM to 3:00 PM) at 2 weeks after virus injection and after overnight fasting (9:30 PM to 8:30 AM) at 4 weeks after virus injection using an OneTouch Select Plus glucose meter (LifeScan, Inc., Milpitas, CA) or an Accu-Chek Performa glucose meter (Roche, Mannheim, Germany). Overnight fasted (9:30 PM to 11:30 AM) animals were euthanized 4 weeks after virus injection for tissue collection. Animals were euthanized by cardiac puncture under isoflurane anesthesia, and tissues were rapidly excised and stored.

For the long-term *G6pc*-targeting experiment, mice were injected with  $0.0/0.5/1.0 \times 10^{11}$  vp sg*G6pc* or EV in  $100 \mu\text{L}$  of sterile PBS. At regular time points during follow-up, mice were fasted overday (8:00 AM to 3:00 PM), after which blood glucose levels were measured as described. At certain time points, sg*G6pc*-treated mice were scanned with MRI (see the Supporting Information for procedures). Two  $1.0 \times 10^{11}$  vp sg*G6pc*-treated animals and two  $0.5 \times 10^{11}$  vp sg*G6pc*-treated animals were euthanized before the end of the study because of humane endpoints (at 55 of 71 and 67 of 68 weeks after virus injection, respectively), yet were included in the analyses. In the final week of the study, the body composition of all animals was analyzed using an LF110 minispec benchtop Time Domain NMR (TD-NMR) analyzer (Bruker, Billerica, MA). Then, 17.5 months after virus injection and after 3.5 hours of fasting (8:30 AM to 12:00 PM), mice were euthanized for tissue collection. Animals were terminated by cardiac puncture under isoflurane anesthesia, tissues were rapidly excised and stored, and hepatic tumors/lesions/cysts were counted, measured, and stored.

For the *G6pc*- and *Chrebpa*-targeting experiments, mice were simultaneously injected with sg*G6pc* ( $0.5 \times 10^{11}$  vp) and three sgRNAs targeting exon 1 of *Chrebpa* (sg*Chrebpa*;  $0.5 \times 10^{11}$  vp) or EV in  $100 \mu\text{L}$  of sterile PBS. Total number of adenoviral particles was adjusted to  $1.0 \times 10^{11}$  vp per animal using EV. Nonfasted animals were euthanized at 8:30 AM for tissue collection 2 weeks after virus injection. Animals were euthanized by cardiac puncture under isoflurane anesthesia, and tissues were rapidly excised and stored.

### ADENOVIRUS GENERATION

Procedures are described in the Supporting Information.

## LIVER HISTOLOGY, BIOCHEMICAL ANALYSIS, AND HEPATIC PROTEOMICS AND LIPOGENIC FLUX ANALYSIS

Procedures are described in the Supporting Information.

## GENE EXPRESSION ANALYSIS AND ANALYSIS OF CRISPR/Cas9 EDITING EFFICIENCY

Total RNA was isolated using TRI-Reagent (Sigma-Aldrich, St. Louis, MO). Coding DNA was obtained by reverse transcription using Moloney Murine Leukemia Virus reverse transcriptase (Invitrogen, Waltham, MA) and amplified using primers and probes listed in Supporting Table S5. mRNA levels were calculated based on a dilution curve of a pool of all samples, expressed relative to cyclophilin/peptidylprolyl isomerase G (*Ppig*, Figs. 2F and 6E) or acidic ribosomal phosphoprotein P0 (*36b4*; Figs. 1B, 4B, and 4G), and normalized to expression level in control animals.

To analyze CRISPR/Cas9 editing efficiency, forward/reverse primer sets were designed for each (set of) sgRNA(s), with the forward primer spanning the predicted site of Cas9 nuclease activity (approximately three nucleotides before the start of the protospacer adjacent motif sequence). When somatic gene editing by CRISPR/Cas9 occurs, inefficient repair will lead to mutations (insertion and deletion of nucleotides, indels) and an inability of the forward primer to bind to this new sequence. A lack of amplified product using these primer sets thus represents efficient editing with that specific (set of) sgRNA(s).

## STATISTICAL ANALYSIS

Data in figures are presented as dot plots with median  $\pm$  interquartile range (IQR), unless stated otherwise. Data in tables are presented as median (range), unless stated otherwise. Data in heatmaps represent z-score normalized values. Statistical analysis was performed using BrightStat ([www.brightstat.com](http://www.brightstat.com)) and GraphPad PRISM software (GraphPad Software Inc., La Jolla, CA). Differences between three or more groups were tested by a two-tailed Kruskal-Wallis H-test, followed by *post hoc* Conover pair-wise comparisons. For analysis of body-weight data and fasting

blood glucose levels in the long-term experiment, we applied a mixed-effects model, which accounts for missing values in repeated-measures ANOVA. For some parameters of the long-term sg*G6pc* study, we did not perform a statistical analysis because of the lack of an appropriate statistical test. For example, the tumor incidence data do not meet the criteria for the chi-squared test, in which all expected values should be  $>1.0$  and  $\geq 20\%$  of the expected values should be  $>5$ . Data on the number of hepatic tumors per mouse are not normally distributed, disqualifying parametric tests; however, given that this type of data also includes many equal ranks, a nonparametric rank-based test (such as the Kruskal-Wallis H-test) was also not suitable. Analysis of the critical point in data on blood glucose levels and plasma TG levels in mice with different hepatic microsomal G6PC activities was performed by fitting a one-phase decay exponential model using nonlinear regression. With the resulting values for the fitted curve and the plateau and its 95% CI, we calculated for which value of G6PC activity the fitted curve would pass through the upper or lower limit of the 95% CI of the plateau. Correlation between plasma TG levels and fasting blood glucose levels was analyzed by Spearman's correlation coefficient.

## Results

### SOMATIC GENE EDITING OF HEPATIC *G6pc* STRONGLY REDUCES HEPATIC G6PC ACTIVITY

To assess whether liver-specific *G6pc* editing induces hepatic GSD-1a in mice,<sup>(3)</sup> we injected hepatocyte-specific, Cas9-expressing C57BL/6J mice with either  $0.5$  or  $1.0 \times 10^{11}$  vp sg*G6pc* (Fig. 1A) and collected plasma and liver tissue at 4 weeks after sg*G6pc* administration. Control mice received an empty adenovirus (EV;  $1.0 \times 10^{11}$  vp). sg*G6pc* treatment reduced the expression of hepatic *G6pc* mRNA, as determined using primers annealing to the sequence targeted by the sgRNAs, by 64% ( $0.5 \times 10^{11}$  vp) and 71% ( $1.0 \times 10^{11}$  vp), as compared to controls (Fig. 1B). Hepatic G6PC protein levels were reduced by 79% and 87% upon administration of  $0.5 \times 10^{11}$  and  $1.0 \times 10^{11}$  vp sg*G6pc*, respectively (Fig. 1B). To examine whether this reduction in G6PC protein

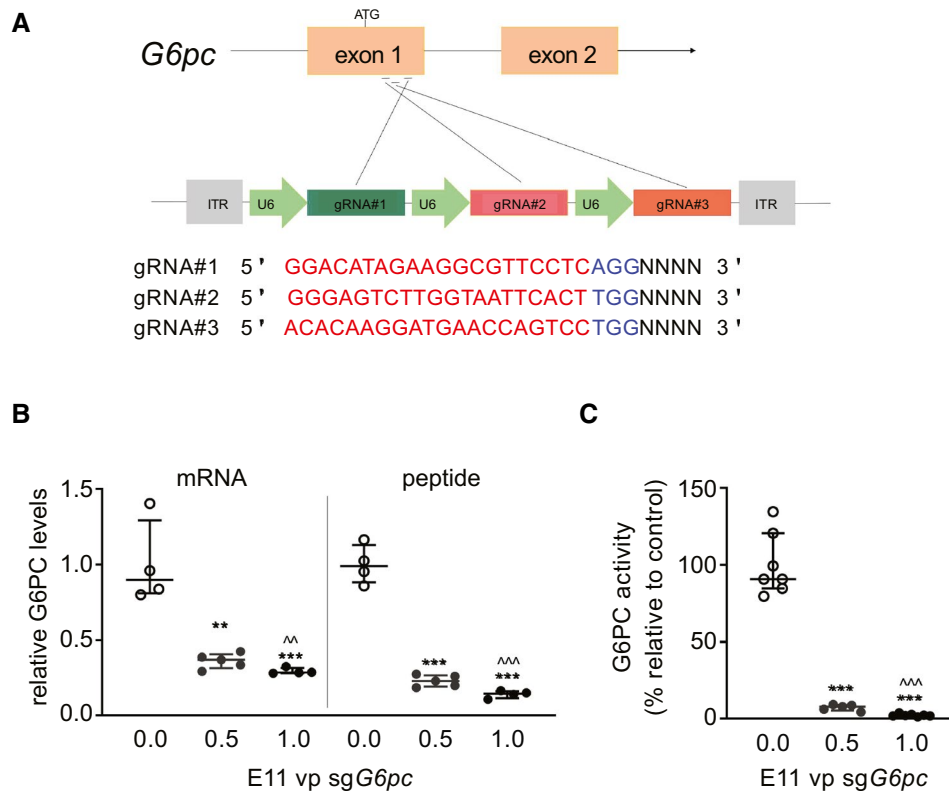


**FIG. 1.** *In vivo* somatic gene editing for hepatic *G6pc* leads to a strong reduction in hepatic G6PC activity. (A) Schematic representation of the single-vector adenoviral system to target *G6pc* in hepatocytes of Cas9-expressing mice. (B) Relative hepatic mRNA levels of *G6pc*, using primers recognizing the sequence edited by sg*G6pc*, and relative protein abundance of G6PC in mice treated with 0.0/0.5/1.0 × 10<sup>11</sup> vp of sg*G6pc*. Total number of adenoviral particles here was not adjusted to 1.0 × 10<sup>11</sup> per animal. (C) Hepatic microsomal G6PC activity in mice treated with 0.0/0.5/1.0 × 10<sup>11</sup> vp of sg*G6pc*, expressed as the percentage (%) relative to the average G6PC activity of animals treated with EV. Data are presented as median ± IQR. Differences between groups were tested by a two-tailed Kruskal-Wallis H-test, followed by *post hoc* Conover pair-wise comparisons. \**P* < 0.05; \*\**P* < 0.01; \*\*\**P* < 0.001, indicates significance compared to 0.0 × 10<sup>11</sup> sg*G6pc* (EV). ^*P* < 0.05; ^^*P* < 0.01; ^^*P* < 0.001, indicates significance compared to 0.5 × 10<sup>11</sup> sg*G6pc*. Abbreviations: ITR, internal terminal repeat.

expression translated into lowered enzymatic activity, we quantified G6PC activity in hepatic microsomal fractions. Hepatic G6PC activity was reduced by ~93% (0.5 × 10<sup>11</sup> vp) and ~98% (1.0 × 10<sup>11</sup> vp) upon sg*G6pc* administration as compared to controls (Fig. 1C).

## HEPATIC *G6pc* EDITING RECAPITULATES GSD-1a BIOCHEMICAL SYMPTOMS

Next, we analyzed biochemical parameters associated with GSD-1a that have an established relationship with impaired G6PC activity in hepatocytes.<sup>(3)</sup> sg*G6pc*-treated mice showed a dose-dependent

reduction in fasting blood glucose levels (Fig. 2A), whereas plasma TG levels increased concomitantly as compared to controls (Fig. 2A). Body weights were similar as compared to controls (Table 1), whereas liver weights were titer-dependently increased at 4 weeks after sg*G6pc* injection (Fig. 2B and Supporting Fig. S1A; Table 1). Food intake and blood glucose levels in the fed state were unaltered (Supporting Fig. S1B,C). These changes recapitulate hypoglycemia and hypertriglyceridemia observed in fasted and poorly controlled GSD-1a patients as well in previously published preclinical GSD-1a models.<sup>(14,23-25,29)</sup> Plasma levels of lactate, uric acid, free fatty acids (FFAs), and total cholesterol were also significantly increased in sg*G6pc*-treated mice, and ketone bodies tended to be

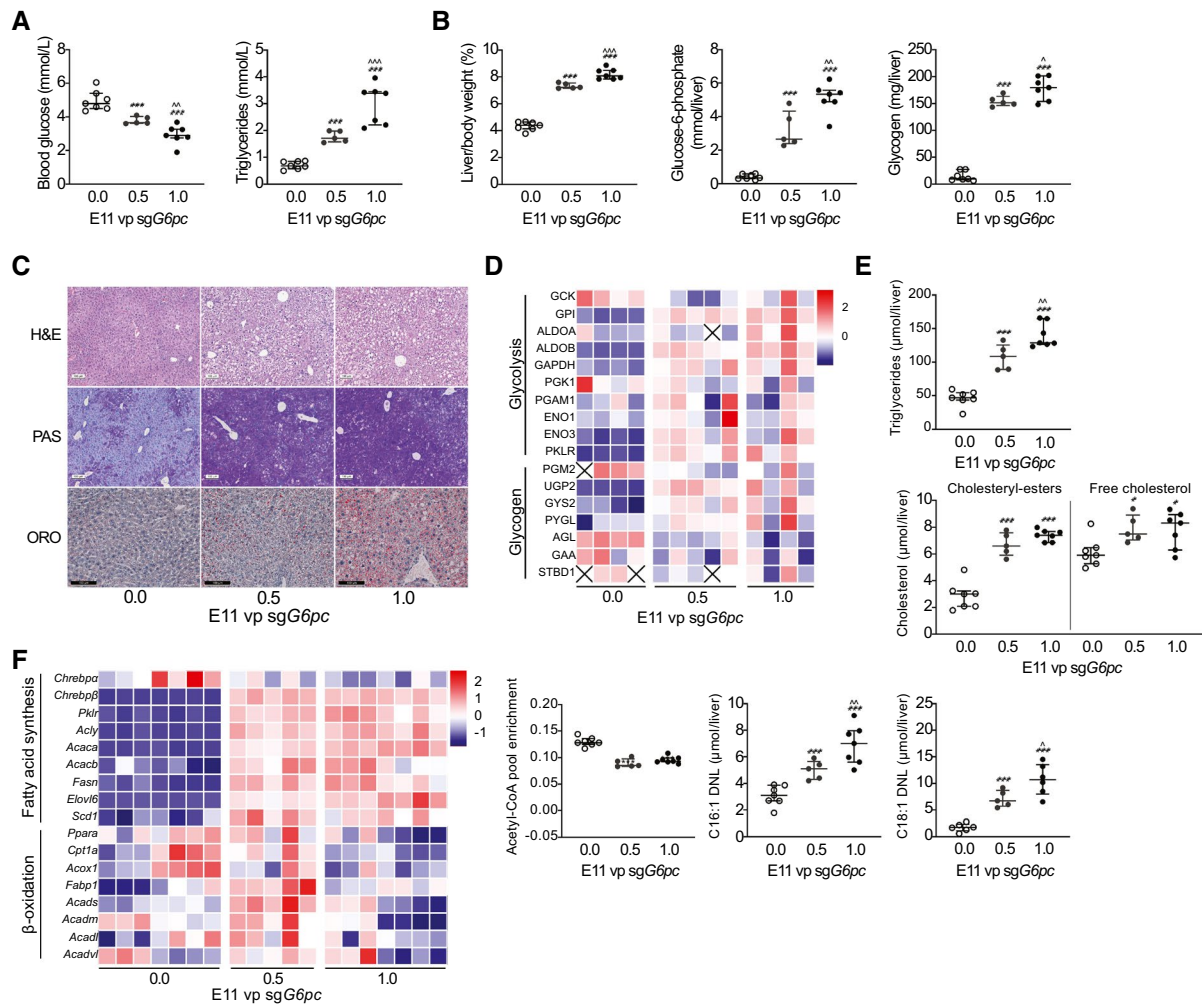


**FIG. 2.** Hepatic *G6pc* editing recapitulates hepatocyte-associated GSD-1a biochemical symptoms. (A) Overnight fasting blood glucose levels and plasma TG levels at 4 weeks after treatment with 0.0/0.5/1.0 × 10<sup>11</sup> vp of *sgG6pc*. (B) Relative liver weight and relative hepatic G6P and glycogen content at 4 weeks after treatment with 0.0/0.5/1.0 × 10<sup>11</sup> vp of *sgG6pc*. (C) Representative photos of H&E, PAS, and ORO stainings of livers of mice treated with 0.0/0.5/1.0 × 10<sup>11</sup> vp of *sgG6pc*. For ORO staining, total number of adenoviral particles was not adjusted to 1.0 × 10<sup>11</sup> per animal. (D) Heatmap presenting z-score normalized peptide levels of proteins involved in glycolysis and glycogen metabolism in mice treated with 0.0/0.5/1.0 × 10<sup>11</sup> vp of *sgG6pc*. Data on GPI, ALDOA, ALDOB, GAPDH, PGK1, ENO1, PKLR, GYS2, PYGL, and AGL represent the average of two peptides (see also Supporting Table S6). Total number of adenoviral particles here was not adjusted to 1.0 × 10<sup>11</sup> per animal. X indicates missing values. (E) Relative hepatic TG, cholesteryl-ester, and free cholesterol content in mice treated with 0.0/0.5/1.0 × 10<sup>11</sup> vp of *sgG6pc*. (F) Left: heatmap presenting z-score normalized mRNA expression levels of hepatic fatty acid synthesis and β-oxidation enzymes in mice treated with 0.0/0.5/1.0 × 10<sup>11</sup> vp of *sgG6pc*. Right: hepatic acetyl-CoA pool enrichment and *de novo* synthesis of palmitate (C16:0) and oleate (C18:1) content in mice treated with 0.0/0.5/1.0 × 10<sup>11</sup> vp of *sgG6pc*. Data are presented as median ± IQR (excluding heatmaps). Differences between groups were tested by a two-tailed Kruskal-Wallis H-test, followed by *post hoc* Conover pair-wise comparisons. \**P* < 0.05; \*\**P* < 0.01; \*\*\**P* < 0.001, indicates significance compared to 0.0 × 10<sup>11</sup> *sgG6pc* (EV). ^*P* < 0.05; ^^*P* < 0.01; ^^*P* < 0.001, indicates significance compared to 0.5 × 10<sup>11</sup> *sgG6pc*. Supporting Table S8A,B contains raw values and statistics for data presented in heatmaps (D,F). Abbreviations: *Acaca*, acetyl-CoA carboxylase 1; *Acacb*, acetyl-CoA carboxylase 2; *Acadl*, acyl-CoA dehydrogenase long chain; *Acadm*, acyl-CoA dehydrogenase medium chain; *Acads*, acyl-CoA dehydrogenase short chain; *Acadvl*, acyl-CoA dehydrogenase very long chain; *Achy*, ATP citrate lyase; *Acox1*, acyl-CoA oxidase 1; ALDOA, aldolase A; ALDOB, aldolase B; AGL, amylo-α-1, 6-glucosidase, 4-α-glucanotransferase; *Cpt1a*, carnitine palmitoyltransferase 1a; DNL, *de novo* lipogenesis; *Elovl6*, ELOVL fatty acid elongase 6; ENO1, enolase 1; ENO3, enolase 3; *Fabp1*, fatty acid binding protein 1; *Fasn*, fatty acid synthase; GAA, alpha glucosidase; GAPDH, glyceraldehyde 3-phosphate dehydrogenase; GPI, glucose-6-phosphate isomerase; GYS2, glycogen synthase 2; PGAM1, phosphoglycerate mutase 1; PGK1, phosphoglycerate kinase 1; PGM2, phosphoglucomutase 2; PKLR, pyruvate kinase L/R; *Ppara*, peroxisome proliferator-activated receptor alpha; PYGL, glycogen phosphorylase L; *Scd1*, stearoyl-CoA desaturase 1; STBD1, starch-binding domain 1; UGP2, UDP-glucose pyrophosphorylase 2.

TABLE 1. Plasma and Liver Parameters of Mice at 4 Weeks After Treatment With *sgG6pc*

Variable	E11 vp <i>sgG6pc</i>		
	0.0	0.5	1.0
Median (Range)			
Body weight (g) night before euthanization	28.1 (25.4-30.3)	28.0 (27.0-28.5)	26.8 (25.5-30.5)
Body weight (g) at euthanization	23.5 (23.3-25.1)	24.2 (23.9-25.9)	25.5 (22.4-26.9)
<b>Plasma</b>			
Lactate (mmol/L)	1.2 (1.0-1.6)	2.2 (1.8-3.0) <sup>‡</sup>	3.5 (1.9-5.3) <sup>‡,§</sup>
Uric acid (mg/L)	25 (22-27)	24 (8-27)	31 (27-34) <sup>*,  </sup>
FFAs (μmol/L)	294 (190-411)	521 (408-580) <sup>‡</sup>	506 (436-671) <sup>‡</sup>
Total ketone bodies (mmol/L)	0.64 (0.37-1.48)	1.00 (0.47-1.45)	0.96 (0.38-1.49)
Total cholesterol (mmol/L)	2.9 (2.3-3.1)	3.6 (2.9-4.5) <sup>†</sup>	3.5 (3.0-4.0) <sup>†</sup>
<b>Liver</b>			
Weight (g)	1.25 (0.96-1.32)	2.00 (1.95-2.15) <sup>‡</sup>	2.25 (2.03-2.39) <sup>‡,  </sup>
G6P (μmol/g liver)	0.28 (0.22-0.47)	1.36 (1.14-2.23) <sup>‡</sup>	2.23 (1.58-2.79) <sup>‡,  </sup>
Glycogen (mg/g liver)	8.4 (5.0-21.3)	74.4 (73.2-79.6) <sup>‡</sup>	79.7 (68.9-87.4) <sup>‡</sup>
TGs (μmol/g liver)	36.4 (20.5-62.2)	50.5 (45.4-66.4) <sup>*</sup>	59.9 (53.6-76.7) <sup>‡</sup>
Total cholesterol (μmol/g liver)	7.10 (6.35-10.55)	7.06 (6.59-7.80)	7.05 (5.83-7.25)
Cholesteryl esters (μmol/g liver)	2.28 (1.61-3.88)	3.31 (2.88-3.66) <sup>*</sup>	3.27 (3.10-3.58) <sup>*</sup>
Free cholesterol (μmol/g liver)	4.92 (4.40-6.67)	3.75 (3.53-4.36) <sup>‡</sup>	3.66 (2.65-3.98) <sup>‡</sup>
Phospholipids (μmol/g liver)	22.5 (22.0-34.6)	17.9 (15.3-19.8) <sup>†</sup>	19.0 (17.2-19.2) <sup>*</sup>
Phospholipids (μmol/liver)	29.7 (27.3-44.6)	35.6 (30.6-42.1)	43.7 (38.6-45.9)
C16:0 fractional DNL (%)	6.0 (3.4-7.4)	7.0 (5.7-7.9)	9.4 (6.1-11.6) <sup>†</sup>
C16:0 DNL (μmol/g liver)	2.4 (1.9-3.0)	2.5 (2.2-2.7)	3.1 (2.5-3.9)
C16:0 OLD (μmol/g liver)	43.7 (35.9-52.6)	33.2 (29.9-36.3) <sup>†</sup>	31.3 (21.6-41.1) <sup>†</sup>
C16:0 OLD (μmol/liver)	53.9 (39.9-58.6)	67.9 (58.3-72.6) <sup>†</sup>	74.5 (51.5-88.9) <sup>‡</sup>
C18:1 fractional DNL (%)	3.1 (1.2-4.4)	4.0 (3.5-5.0) <sup>*</sup>	5.1 (3.3-6.7) <sup>‡</sup>
C18:1 fractional CE (%)	3.1 (2.2-3.6)	5.5 (3.0-7.2) <sup>*</sup>	6.8 (6.0-9.1) <sup>‡,§</sup>
C18:1 DNL (μmol/g liver)	1.4 (0.7-2.2)	3.4 (2.8-4.3) <sup>‡</sup>	4.6 (3.2-6.3) <sup>‡,§</sup>
C18:1 CE (μmol/g liver)	1.5 (0.9-1.8)	4.0 (2.8-5.6) <sup>‡</sup>	6.3 (4.4-11.6) <sup>‡,  </sup>
C18:1 CE (μmol/liver)	1.9 (1.0-2.4)	7.8 (5.7-10.9) <sup>‡</sup>	13.5 (10.5-25.0) <sup>‡,¶</sup>
C18:1 OLD (μmol/g liver)	45.9 (34.0-52.0)	77.8 (63.9-89.9) <sup>†</sup>	83.8 (45.0-109.4) <sup>†</sup>
C18:1 OLD (μmol/liver)	56.2 (37.8-62.7)	166.2 (124.5-179.9) <sup>‡</sup>	186.3 (107.7-236.4) <sup>‡</sup>
Histological scores derived from H&E			
Glycogen vacuolopathy <sup>#</sup>	1 (1-2)	3 (3-3)	3 (3-3)
Lobular inflammation <sup>**</sup>	2 (0-3)	1 (0-1)	1 (0-1)
Single cell death <sup>††</sup>	1 (0-1)	0 (0-1)	0 (0-4)

\*  $P < 0.05$ , indicates significance compared to 0.0 E11 vp *sgG6pc*.

†  $P < 0.01$ , indicates significance compared to 0.0 E11 vp *sgG6pc*.

‡  $P < 0.001$ , indicates significance compared to 0.0 E11 vp *sgG6pc*.

§  $P < 0.05$ , indicates significance compared to 0.5 E11 vp *sgG6pc*.

||  $P < 0.01$ , indicates significance compared to 0.5 E11 vp *sgG6pc*.

¶  $P < 0.001$ , indicates significance compared to 0.5 E11 vp *sgG6pc*.

# Semiquantitative scores. 0: <5%; 1: 5%–33%; 2: 33%–66%; 3: >66%.

\*\* Semiquantitative scores. 0: none; 1: <2 foci per 200× field; 2: 2–4 foci per 200× field; 3: >4 foci per 200× field.

†† Number of single cell deaths in five 200× fields.

Abbreviations: DNL, *de novo* lipogenesis; CE, chain elongation.

elevated (Table 1). Consistent with reduced hepatic G6PC activity, hepatic G6P and glycogen contents were increased in a *sgG6pc* titer-dependent fashion (Fig. 2B; Table 1). Increases in hepatic glycogen content were confirmed by higher periodic acid Schiff

(PAS) staining (Fig. 2C) and associated with increased hepatocyte vacuolopathy as shown by hematoxylin and eosin (H&E) staining (Fig. 2C; Table 1). *sgG6pc* treatment did not affect hepatic inflammation, single cell death, or fibrosis (Table 1; Supporting Fig. S1D).

The reduction in hepatic G6PC levels and activity in sg*G6pc*-treated mice was paralleled by increased protein expression of most glycolytic enzymes, whereas enzymes involved in glycogen metabolism, such as UDP-glucose pyrophosphorylase 2 (UGP2), glycogen synthase 2 (GYS2), and glycogen phosphorylase L (PYGL), tended to be increased (Fig. 2D). In addition, Oil Red O (ORO) staining showed increased neutral lipid storage upon sg*G6pc* treatment (Fig. 2C), in agreement with increased hepatic TG and cholesteryl ester contents (Fig. 2E; Table 1). Hepatic free cholesterol and hepatic phospholipid contents were reduced in sg*G6pc*-treated mice compared to controls (Table 1), whereas total hepatic free cholesterol content was slightly increased because of increased liver weight (Fig. 2E; Table 1). The increases in hepatic TG and cholesteryl ester content were paralleled by increased hepatic mRNA levels of genes involved in glycolysis and *de novo* lipogenesis (Fig. 2F) as well as by reduced hepatic acetyl-CoA pool enrichment (a measure for acetyl-CoA pool turnover; Fig. 2F), increased *de novo* synthesis of palmitate (C16:0) and oleate (C18:1; Fig. 2F), and increased elongation of pre-existing palmitate to oleate (Table 1). sg*G6pc*-treated mice showed an increase in hepatic stearate, vaccinate, and oleate contents, whereas eicosapentanoate, docosapentanoate, and docosahexanoate levels were reduced (Supporting Table S1). Hepatic mRNA levels of genes involved in fatty acid oxidation tended to be increased by  $0.5 \times 10^{11}$  vp of sg*G6pc* and normalized by  $1.0 \times 10^{11}$  vp of sg*G6pc* (Fig. 2F).

## HEPATIC *G6pc* EDITING PERMANENTLY INDUCES FASTING HYPOGLYCEMIA AND CAUSES LIVER TUMOR DEVELOPMENT

To examine whether long-term hepatic *G6pc* editing results in liver tumor development, we performed a 75-week follow-up of  $0.5$  and  $1.0 \times 10^{11}$  vp sg*G6pc*-treated mice and controls. This follow-up period corresponds to 40–45 years in humans, an age at which >70% of GSD-1a patients have developed liver tumors.<sup>(4)</sup> Starting ~20 weeks after sg*G6pc* administration, mice injected with  $1.0 \times 10^{11}$  vp sg*G6pc* showed a significantly lower body weight as compared to controls (Fig. 3A). Body composition analysis revealed that sg*G6pc*-treated mice exhibited a significant reduction in

absolute fluid and lean mass and a lower relative fluid mass as compared to control mice (Table 2). To validate that fasting hypoglycemia persisted over time, fasting blood glucose levels were repeatedly analyzed. Indeed, fasting blood glucose levels were dose-dependently reduced in sg*G6pc*-treated compared to control mice during the entire follow-up period (Fig. 3A). MRI identified potential sites of liver tumor development at 55 ( $1.0 \times 10^{11}$  vp of sg*G6pc*) and 68 weeks ( $0.5 \times 10^{11}$  vp of sg*G6pc*) post-sg*G6pc* administration (Fig. 3B). At 75 weeks post-sgRNA administration, sg*G6pc*-treated mice showed lower body weights, reduced blood glucose levels, and enlarged livers as compared to controls (Table 2; Fig. 3B). The total number and relative incidence of hepatic tumors of different sizes (Fig. 3C,D; Table 2), as well as the incidence and number of hepatocellular carcinoma (HCC) per mouse (Fig. 3C; Table 2), tended to be increased in sg*G6pc*-treated mice. In addition, the average number of hepatic tumors (hepatocellular carcinoma [HCA], HCC, and hepatoblastoma [HB]; Fig. 3C) tended to be increased in sg*G6pc*-treated mice. Immunohistochemical stainings indicated that HB showed reduced alpha-fetoprotein (AFP), hepatocyte paraffin 1 (Heppar1), and cytokeratin 19 (CK19) and comparable glypican-3 (GPC3) expression as compared to nontumor tissue (Supporting Fig. S2). Moreover, HCA and HCC sections showed variable staining for AFP and reduced CK19 staining. GPC3 and Heppar1 stainings were variable in HCA, whereas they were increased in HCC sections (Supporting Fig. S2).

## HEPATIC CRISPR/Cas9-MEDIATED GENE EDITING ENABLES SIMULTANEOUS MANIPULATION OF HEPATIC *G6pc* AND MLX-INTERACTING PROTEIN-LIKE

To explore whether our approach allows for simultaneous *in vivo* editing of multiple hepatic candidate genes in GSD-1a, we coadministered sgRNAs against *G6pc* and MLX-interacting protein-like (*Mlxip*; Fig. 4A). The latter gene encodes ChREBP $\alpha$ , a glucose-sensitive transcription factor that is activated in GSD-1a and protects against fatty liver development in hepatocyte-specific *G6pc*-knockout mice.<sup>(13)</sup> Two weeks after sgRNA administration, we confirmed efficient editing of both hepatic *G6pc* and *Chrebp $\alpha$*



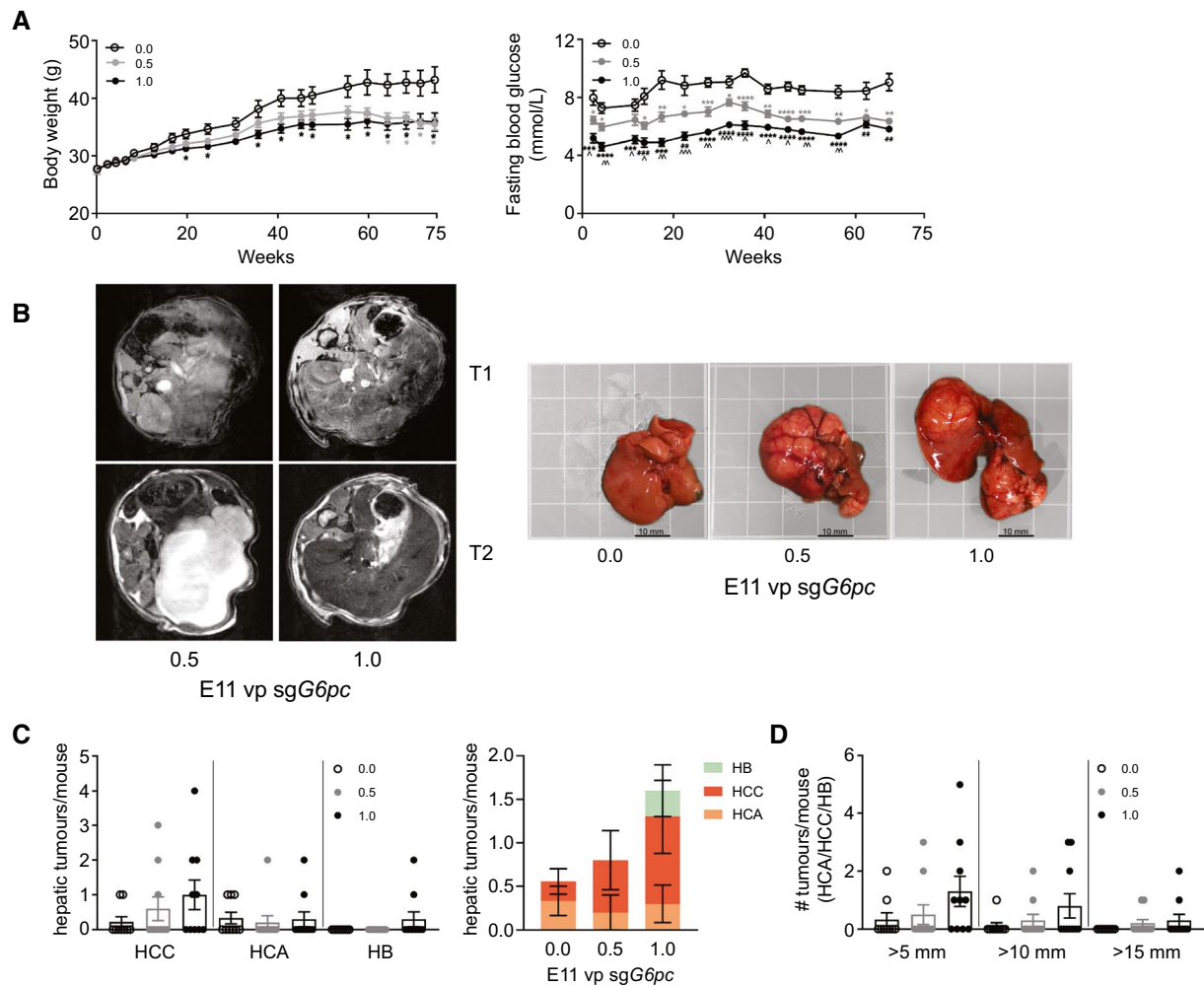


**FIG. 3.** Hepatic *G6pc* editing permanently induces fasting hypoglycemia and promotes liver tumor development. (A) Left: body weight of mice treated with 0.0/0.5/1.0  $\times 10^{11}$  vp of *sgG6pc* at 0–75 weeks after *sgG6pc* treatment. Right: overnight fasting blood glucose levels at 2–67 weeks after treatment with 0.0/0.5/1.0  $\times 10^{11}$  vp of *sgG6pc*. Statistical significance was tested by using a mixed-effects model, which accounts for missing values in repeated-measures ANOVA. Data are presented as mean  $\pm$  SEM. \* $P < 0.05$ ; \*\* $P < 0.01$ ; \*\*\* $P < 0.001$ , indicates significance compared to 0.0  $\times 10^{11}$  *sgG6pc* (EV). ^ $P < 0.05$ ; ^^ $P < 0.01$ ; ^^ $P < 0.001$ , indicates significance compared to 0.5  $\times 10^{11}$  *sgG6pc*. (B) Left: representative macroscopical T<sub>1</sub>- and T<sub>2</sub>-weighted MRI images (at 68 and 55 weeks after *sgG6pc* treatment, respectively). Right: representative macroscopical liver photos at 75, 67, and 71 weeks after *sgG6pc*/EV treatment, respectively. (C) Left: quantification of the number of HCCs, HCAs, and HBs per mouse in mice 55–75 weeks after treatment with 0.0/0.5/1.0  $\times 10^{11}$  vp of *sgG6pc*. Right: mean number of HCCs/HCAs/HBs per group. Data are presented as mean  $\pm$  SEM. (D) Quantification of the number of hepatic tumors (HCA, HCC, and HB) >5, >10, and >15 mm per mouse in mice 55–75 weeks after treatment with 0.0/0.5/1.0  $\times 10^{11}$  vp of *sgG6pc*. Data are presented as mean  $\pm$  SEM. (C,D) Statistical significance was not tested because of the lack of an appropriate statistical test (see Materials and Methods).

(Fig. 4B). Moreover, the induced hepatic *Chrebpb* mRNA levels in *sgG6pc*-treated mice were normalized to values observed in controls after receiving the combination of *sgG6pc* and *sgChrebpa* (Fig. 4B). Consistent with our previous work,<sup>(13)</sup> simultaneous editing of hepatic *G6pc* and *Chrebpa* induced more severe hepatomegaly as compared to *sgG6pc* treatment

alone, as shown by further increases in liver weight (Fig. 4C,E; Supporting Table S2), hepatic G6P and glycogen contents (Fig. 4D; Supporting Table S2), and hepatocyte vacuolopathy (Fig. 4E). Simultaneous editing of hepatic *G6pc* and *Chrebpa* also further increased hepatic TG content (Fig. 4F) and normalized lipogenic gene expression (Fig. 4G).

TABLE 2. Mouse Characteristics of Mice at 55-76 Weeks After Treatment With sgG6pc

Variable	E11 vp sgG6pc		
	0.0	0.5	1.0
Median (Range)			
Humane endpoint before end of study (weeks)	0 cases	2 cases: 67, 68	2 cases: 55, 71
Body weight at euthanization (g)	41.8 (33.6-50.2)	34.6 (28.0-40.8)*	35.1 (24.2-41.9)*
O/D fasted blood glucose (mmol/L)	7.6 (6.3-8.4)	5.5 (4.8-6.5) <sup>‡</sup>	4.9 (3.8-6.3) <sup>‡</sup>
Lean mass (g)	25.8 (23.2-27.7)	23.9 (22.1-24.8) <sup>†</sup>	24.5 (19.3-25.4)*
Fluid mass (g)	4.1 (3.0-5.3)	2.9 (2.4-3.7) <sup>†</sup>	3.0 (1.8-3.9) <sup>†</sup>
Fat mass (g)	13.7 (4.0-20.2)	7.9 (2.5-11.8)	8.3 (2.8-14.5)
Lean mass (%)	59.4 (50.6-74.4)	68.8 (61.3-82.0)	68.1 (57.2-80.9)
Fluid mass (%)	9.6 (8.6-14.0)	8.7 (7.3-10.2)*	8.7 (7.4-9.3)*
Fat mass (%)	31.2 (11.6-39.1)	22.7 (8.9-30.0)	22.8 (11.7-33.8)
<b>Liver</b>			
Weight (g; including tumor mass)	1.9 (1.3-2.9)	2.4 (2.1-6.3)*	2.9 (2.4-7.1) <sup>‡</sup>
Liver/body weight ratio (%; including tumor mass)	4.9 (3.7-5.7)	6.8 (5.9-22.6) <sup>‡</sup>	7.7 (7.1-22.1) <sup>‡,§</sup>
<b>Liver tumors/lesions/cysts</b>			
Relative incidence HCA/HCC/HB <sup>#,***</sup>	33%	30%	70%
<i>By category</i>			
Relative incidence HCA <sup>#</sup>	33%	10%	20%
Relative incidence HCC <sup>#,***</sup>	22%	30%	50%
Relative incidence HB <sup>#</sup>	0%	0%	20%
<i>By size, mm</i>			
>5 <sup>††</sup>	22%	20%	60%
>10 <sup>††</sup>	11%	20%	30%
>15 <sup>††</sup>	0%	20%	20%

\*  $P < 0.05$ , indicates significance compared to 0.0 E11 vp sgG6pc.

<sup>†</sup>  $P < 0.01$ , indicates significance compared to 0.0 E11 vp sgG6pc.

<sup>‡</sup>  $P < 0.001$ , indicates significance compared to 0.0 E11 vp sgG6pc.

<sup>§</sup>  $P < 0.05$ , indicates significance compared to 0.5 E11 vp sgG6pc.

<sup>||</sup>  $P < 0.01$ , indicates significance compared to 0.5 E11 vp sgG6pc.

<sup>¶</sup>  $P < 0.001$ , indicates significance compared to 0.5 E11 vp sgG6pc.

<sup>#</sup> Percentage of mice with at least one HCA, one HCC, or one HB lesion according to histological classification.

<sup>\*\*\*</sup> Three lesions were a mixture of HCA and HCC. In all these cases, the lesion was classified as HCC, and not as HCA.

<sup>††</sup> Percentage of mice with at least one lesion, histologically classified as HCA, HCC, or HB, larger than 5/10/15 mm in diameter.

Abbreviation: O/D, overday.

## HEPATIC GENE EDITING USING CRISPR/Cas9 ALLOWS FOR GENERATING A SPECTRUM OF HEPATIC GSD-1a PHENOTYPES

We finally performed a sgG6pc dosing study to model the phenotypic heterogeneity observed in GSD-1a patients,<sup>(11)</sup> which is proposedly partially related to variations in residual G6PC activity between 0% and 23%.<sup>(2,6,11,26)</sup> For this purpose, we injected hepatocyte-specific, Cas9-expressing mice with various amounts of sgG6pc or control virus and evaluated GSD-1a-associated biochemical symptoms after 4 weeks. This approach generated a spectrum

of hepatic G6PC activities ranging from 1% to 108% compared to average control values, with a clear titer-dependent reduction in residual activity (Supporting Fig. S3A). We subsequently classified mice into groups with either >60%, 20%-60%, 10%-20%, 5%-10%, or <5% residual hepatic G6PC activities. Reductions in hepatic G6PC activity were paralleled by dose-dependent decreases in fasting blood glucose levels (Fig. 5A). Nonlinear regression analysis showed a plateau blood glucose value of 4.875 mmol/L (Fig. 5B, dashed lines; 95% CI, 4.574-5.200), and that hepatic G6PC activities <~20% resulted in significant reductions of blood glucose levels as compared to this plateau value (Fig. 5B, red dot). Fasting

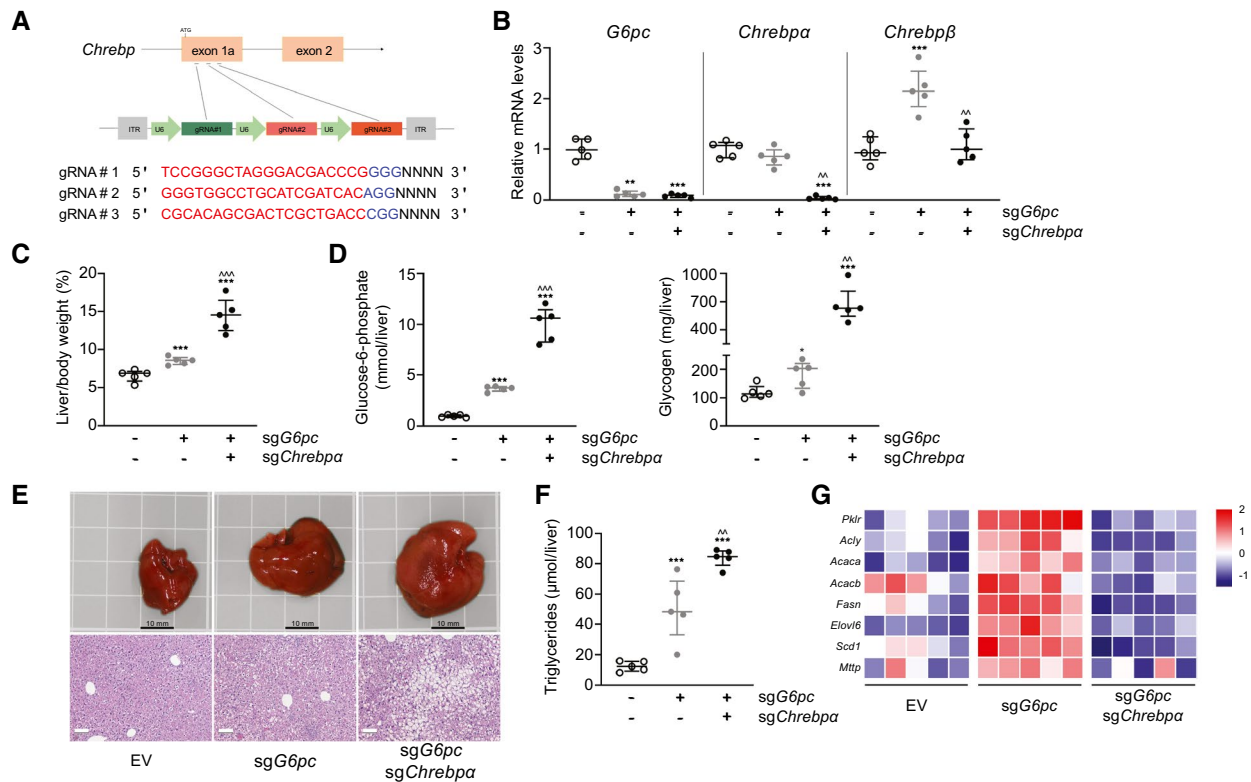


**FIG. 4.** Hepatic CRISPR/Cas9-mediated gene editing enables simultaneous manipulation of hepatic *G6pc* and *Mlxipl*. (A) Schematic representation of the single-vector adenoviral system to target *Mlxipl* (*Chrebp*) in hepatocytes of Cas9-expressing mice. (B) Left: relative hepatic mRNA levels of *G6pc* and *Chrebp* $\alpha$ , using primers recognizing the sequence edited by *sgG6pc* and *sgChrebp* $\alpha$ , in mice treated with *sgG6pc* and with/without *sgChrebp* $\alpha$ . Right: normalized relative hepatic *Chrebp* $\beta$  mRNA levels in mice treated with *sgG6pc* and with/without *sgChrebp* $\alpha$ . (C) Relative liver weight in mice treated with *sgG6pc* and with/without *sgChrebp* $\alpha$ . (D) Relative hepatic G6P and glycogen content in mice treated with *sgG6pc* and with/without *sgChrebp* $\alpha$ . (E) Representative macroscopical liver photos and H&E stainings of liver sections from mice treated with *sgG6pc* and with/without *sgChrebp* $\alpha$ . (F) Relative hepatic TG content in mice treated with *sgG6pc* and with/without *sgChrebp* $\alpha$ . (G) Heatmap presenting z-score normalized mRNA expression levels of hepatic fatty acid synthesis and TG synthesis enzymes in mice treated with *sgG6pc* and with/without *sgChrebp* $\alpha$ . Data are presented as median  $\pm$  IQR (excluding heatmap). Differences between groups were tested by a two-tailed Kruskal-Wallis H-test, followed by *post hoc* Conover pair-wise comparisons. \* $P < 0.05$ ; \*\* $P < 0.01$ ; \*\*\* $P < 0.001$ , indicates significance compared to EV-treated mice. ^ $P < 0.05$ ; ^^ $P < 0.01$ ; ^^ $P < 0.001$ , indicates significance compared to *sgG6pc*-treated mice. Abbreviations: *Acaca*, acetyl-CoA carboxylase 1; *Acacb*, acetyl-CoA carboxylase 2; *Acl*, ATP citrate lyase; *Elovl6*, ELOVL fatty acid elongase 6; *Fasn*, fatty acid synthase; gRNA, guide RNA; ITR, inverted terminal repeats; *Mttp*, microsomal triglyceride transfer protein; *Pklr*, pyruvate kinase L/R; *Scd1*, stearoyl-CoA desaturase 1.

plasma TG levels were titer-dependently increased upon *sgG6pc* administration (Fig. 5A), with a plateau value of 0.658 mmol/L (Fig. 5B, dashed lines; 95% CI, 0.3995–0.9064), and with hepatic G6PC activities below  $\sim 24\%$  resulting in significant increases of plasma TG levels as compared to the plateau value (Fig. 5B, red dot). Plasma TG levels were inversely correlated to fasting blood glucose levels (Supporting Fig. S3B).

## VARIATIONS IN RESIDUAL HEPATIC G6PC ACTIVITY TRANSLATE INTO SEVERITY OF HEPATOMEGALY AND HEPATIC G6P AND GLYCOGEN ACCUMULATION

We also investigated the impact of variable residual hepatic G6PC activities on hepatomegaly.

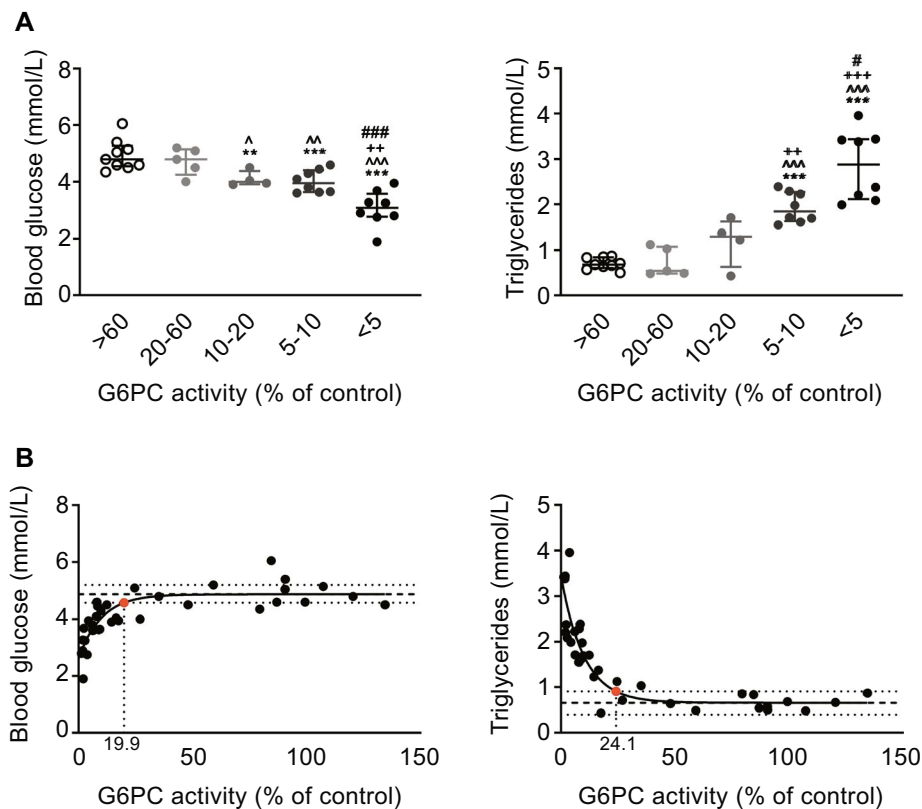


**FIG. 5.** *sgG6pc* administration dose-dependently induces fasting hypoglycemia and hypertriglyceridemia. (A) Overnight fasting blood glucose levels and plasma TG levels in mice with different hepatic microsomal G6PC activities attributable to *sgG6pc* treatment. (B) Left: fasting blood glucose level plotted against hepatic microsomal G6PC activity. Nonlinear regression showed a plateau blood glucose value of 4.875 mmol/L (dashed line) with a 95% CI of 4.574–5.200 (dotted lines), and that a hepatic G6PC activity  $\sim$ 20% resulted in a significant reduction of the blood glucose value as compared to this plateau value (red dot, intersection of nonlinear fit-curve and 95% CI). Right: fasting plasma TG level plotted against hepatic microsomal G6PC activity. Nonlinear regression showed a plateau plasma TG level of 0.658 mmol/L (dashed line), with a 95% CI of 0.3995–0.9064 (dotted lines), and that a hepatic G6PC activity  $\sim$ 24% resulted in a significant increase of plasma TG levels as compared to this plateau value (red dot, intersection of nonlinear fit-curve and 95% CI). Data in (A) are presented as median  $\pm$  IQR. Differences between groups were tested by a two-tailed Kruskal-Wallis H-test, followed by *post hoc* Conover pair-wise comparisons. \* $P < 0.05$ ; \*\* $P < 0.01$ ; \*\*\* $P < 0.001$ , indicates significance compared to mice with  $>60\%$  G6PC activity. ^ $P < 0.05$ ; ^^ $P < 0.01$ ; ^^^ $P < 0.001$ , indicates significance compared to mice with 20%–60% G6PC activity. \* $P < 0.05$ ; \*\* $P < 0.01$ ; \*\*\* $P < 0.001$ , indicates significance compared to mice with 10%–20% G6PC activity. # $P < 0.05$ ; ## $P < 0.01$ ; ### $P < 0.001$ , indicates significance compared to mice with 5%–10% G6PC activity. G6PC activity control value (x-axis) is the average activity in mice treated with EV.

Individual mice exhibiting  $<60\%$  residual hepatic G6PC activity showed activity-dependent increases in liver weight, whereas body weight was not affected (Fig. 6A; Supporting Table S3). This was associated with more pronounced hepatocyte vacuolopathy (Fig. 6B) and activity-dependent increases in hepatic G6P and glycogen contents (Fig. 6C). Moreover, residual hepatic G6PC activities below  $\sim 41\%$  resulted in hepatic TG and cholesteryl ester accumulation (Fig. 6D and Supporting Fig. S3C; Supporting Table S3). Increased mRNA levels of

enzymes involved in glycolysis and *de novo* lipogenesis, reduced hepatic acetyl-CoA pool enrichments, increased *de novo* synthesis of palmitate (C16:0) and oleate (C18:1), increased elongation of pre-existing palmitate to oleate, and increased hepatic concentrations of oleate were also observed in an activity-dependent fashion (Fig. 6E–F; Supporting Tables S3 and S4). Hepatic mRNA levels of fatty acid oxidation enzymes tended to be increased upon *sgG6pc* treatment up to  $\sim 5\%$  residual activity, after which they normalized (Fig. 6E).

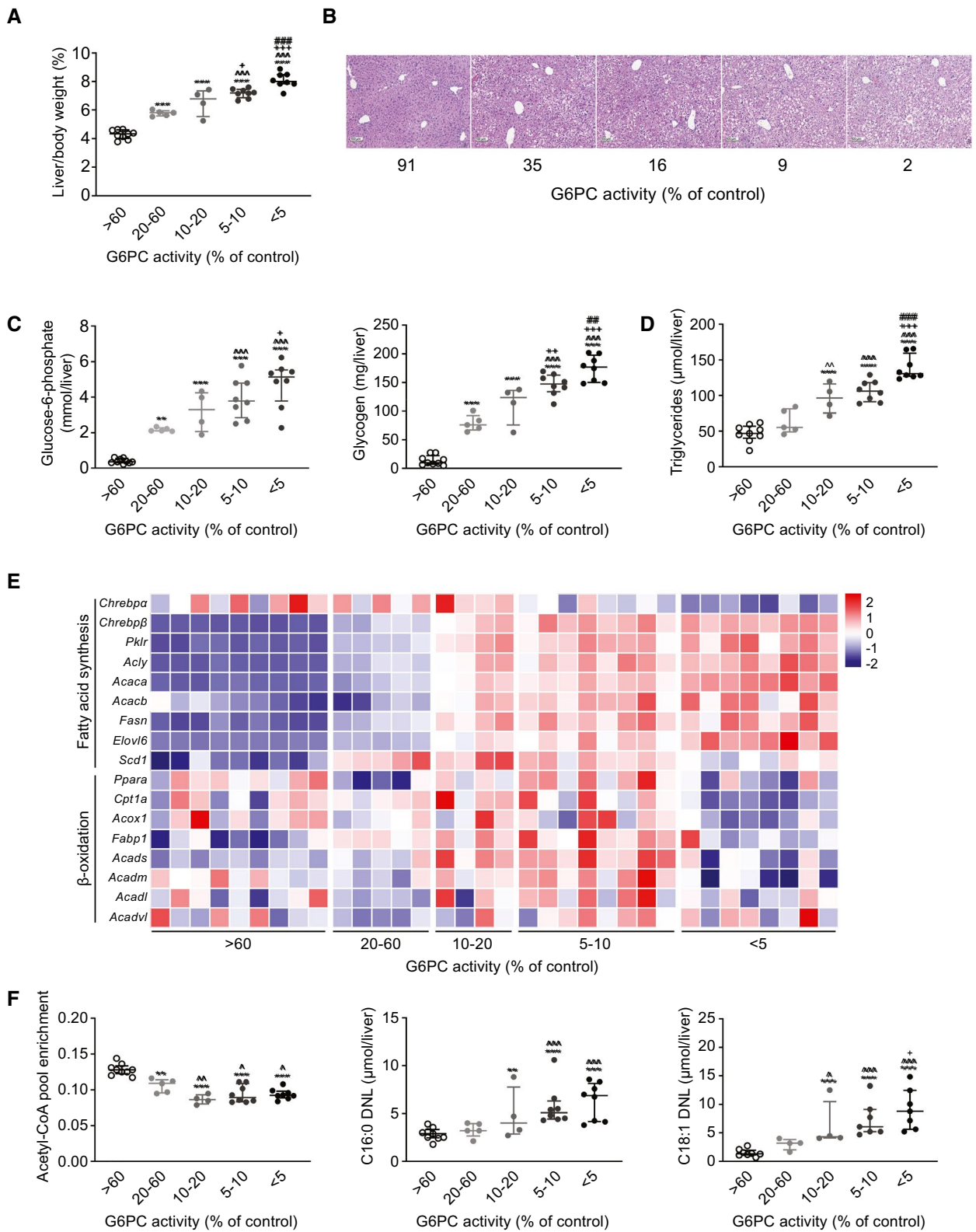


**FIG. 6.** *sgG6pc* administration dose-dependently induces hepatomegaly and hepatic metabolite accumulation. (A) Relative liver weight in mice with different hepatic microsomal G6PC activities attributable to *sgG6pc* treatment. (B) Representative photos of H&E staining of livers of mice with different hepatic microsomal G6PC activities attributable to *sgG6pc* treatment. (C) Relative hepatic G6P and glycogen content in mice with different hepatic microsomal G6PC activities attributable to *sgG6pc* treatment. (D) Relative hepatic TG content in mice with different hepatic microsomal G6PC activities attributable to *sgG6pc* treatment. (E) Heatmap presenting z-score normalized mRNA expression levels of hepatic fatty acid synthesis and  $\beta$ -oxidation enzymes in mice with different hepatic microsomal G6PC activities attributable to *sgG6pc* treatment. (F) Hepatic acetyl-CoA pool enrichment and *de novo* synthesis of palmitate (C16:0) and oleate (C18:1) content in mice with different hepatic microsomal G6PC activities attributable to *sgG6pc* treatment. Data are presented as median  $\pm$  IQR (except heatmap). Differences between groups were tested by a two-tailed Kruskal-Wallis H-test, followed by *post hoc* Conover pairwise comparisons. \* $P < 0.05$ ; \*\* $P < 0.01$ ; \*\*\* $P < 0.001$ , indicates significance compared to mice with >60% G6PC activity.  $^{\wedge}P < 0.05$ ;  $^{\wedge\wedge}P < 0.01$ ;  $^{\wedge\wedge\wedge}P < 0.001$ , indicates significance compared to mice with 20%–60% G6PC activity. \* $P < 0.05$ ; \*\* $P < 0.01$ ; \*\*\* $P < 0.001$ , indicates significance compared to mice with 10%–20% G6PC activity.  $^{\#}P < 0.05$ ;  $^{\#\#}P < 0.01$ ;  $^{\#\#\#}P < 0.001$ , indicates significance compared to mice with 5%–10% G6PC activity. G6PC activity control value (x-axis) is the average activity in mice treated with EV. Supporting Table S8C contains raw values and statistics for data presented in the heatmap (E). Abbreviations: *Acaca*, acetyl-CoA carboxylase 1; *Acacb*, acetyl-CoA carboxylase 2; *Acadl*, acyl-CoA dehydrogenase long chain; *Acadm*, acyl-CoA dehydrogenase medium chain; *Acads*, acyl-CoA dehydrogenase short chain; *Acadol*, acyl-CoA dehydrogenase very long chain; *Acly*, ATP citrate lyase; *Acox1*, acyl-CoA oxidase 1; *Cpt1a*, carnitine palmitoyltransferase 1a; DNL, *de novo* lipogenesis; *Elovl6*, ELOVL fatty acid elongase 6; *Fabp1*, fatty acid binding protein 1; *Fasn*, fatty acid synthase; *Pklr*, pyruvate kinase L/R; *Ppara*, peroxisome proliferator-activated receptor alpha; *Scd1*, stearoyl-CoA desaturase 1.

## Discussion

In the current study, we successfully used somatic CRISPR/Cas9-mediated gene editing to generate a mouse model for hepatic GSD-1a. This approach recapitulates the key biochemical symptoms of GSD-1a, hepatomegaly, and liver tumor formation. We also show that it allows one to efficiently study GGIs and, importantly, to model phenotypic heterogeneity observed in GSD-1a patients.

Heterogeneity in biochemical symptoms and long-term complications and limited insight into the molecular mechanisms underlying liver tumor development pose major challenges to the long-term health of GSD-1a patients.<sup>(12)</sup> Here, we report that mice with <60% hepatic G6PC activity displayed hepatomegaly and enhanced hepatic glycogen storage, hyperlactatemia, hepatic ChREBP activation, acetyl-CoA pool turnover, as well as a slight increase in *de novo* oleate synthesis. These changes are most likely attributable to hepatic G6P accumulation, excess glycogen storage, and enhanced glycolysis. On the other hand, fasting hypoglycemia, hypertriglyceridemia, and hepatic steatosis (HS) were evident only in mice with <25%–40% G6PC activity. These results are in line with data from full-body *G6pc*-null mice and hepatocyte-specific *G6pc*-knockout mice that received *G6pc* gene therapy.<sup>(30–33)</sup> In addition, our findings are consistent with the phenotype of heterozygous *G6pc*-null mice, which do not show fasting hypoglycemia or hypertriglyceridemia.<sup>(23)</sup> The correlation between

hypertriglyceridemia/HS and hypoglycemia in the current study further supports our previous work showing that hypoglycemia in hepatocyte-specific, G6PC-deficient mice arrests VLDL-TG catabolism and enhances hepatic FFA influx, resulting in more pronounced hypertriglyceridemia and HS.<sup>(34)</sup> Taken together, we propose that the relationship between hepatic G6PC activity and hypertriglyceridemia and HS is predominantly determined by the degree of hypoglycemia, rather than solely dependent on enhanced intrahepatic glycolysis and *de novo* lipogenesis.

Recent studies from several laboratories including ours have generated insights in transcriptional and posttranscriptional dysregulation of biochemical pathways in GSD-1a mouse models.<sup>(13–17,21,22)</sup> Yet, our approach has several advantages over existing models, given that it allows the systematic investigation of the contribution of distinct genes and their target pathways to disease symptoms and complications *in vivo*. The successful concomitant knockdown of hepatic *G6pc* and *Chrebp*a in the current study confirms that multiple gene editing *in vivo* is feasible in mice using CRISPR/Cas9 technology.<sup>(35,36)</sup> As a result, cross-breeding of genetically modified mice, as well as repetitive administration of short hairpin RNAs or antisense oligonucleotides, either or not in combination with tamoxifen injections,<sup>(14,24)</sup> can be avoided.<sup>(35,36)</sup> This reduces labor-, time-, and cost-intensive experimentation while, at the same time, limiting animal discomfort.

A number of features related to our approach warrant discussion. First, glucose production by kidney cells and enterocytes,<sup>(3,37,38)</sup> which is impaired in GSD-1a patients, is presumably increased in sg*G6pc*-treated mice to compensate for reduced hepatic G6PC activity.<sup>(37,38)</sup> Moreover, whereas GSD-1a patients depend on dietary complex carbohydrates to maintain euglycemia during day and night, sg*G6pc*-treated mice do not consume additional carbohydrates during their (inactive) phase when lights are on. Although these differences between mouse models and patients may complicate a direct comparison between residual hepatic G6PC activity and GSD-1a heterogeneity, it is also a well-known limitation of other liver-specific GSD-1a mouse models. Second, we observed a higher prevalence of hepatic nodules/tumors in our control group, as compared to C57BL/6J mice in the Mouse Tumor Biology (MTB) database,<sup>(39)</sup> and found larger (>10 mm) nodules in our study in comparison to published mouse models for hepatic GSD-1a.<sup>(24,25)</sup> We hypothesize that, in addition to aging-induced liver tumor formation,<sup>(40,41)</sup> the use of an adenoviral delivery system<sup>(42-44)</sup> may have resulted in higher tumor incidences in the current study. Further experimental optimization, such as the use of liposome-based sgRNA administration, may offer opportunities to reduce this potential side effect.

Patient-specific differences in residual hepatic G6PC activities and the degree of metabolic control translate into variations in disease symptoms and complications.<sup>(7-11)</sup> Currently available mouse models<sup>(23-25)</sup> do not allow to model such clinical heterogeneity that is typically observed between GSD-1a patients,<sup>(2,6,11,26)</sup> which limits their translational value. In contrast, in the current study, mice treated with different sg*G6pc* doses likely displayed a “mosaic” pattern of hepatocellular G6PC activity as a result of the variety of mutations induced by CRISPR/Cas9<sup>(45)</sup> and the number of hepatocytes edited. The residual hepatic G6PC activities therefore represent “average” values of individual hepatocytes. Interestingly, despite the presumed mosaic pattern of hepatic G6PC activity, the total residual activity per liver clearly correlated with disease symptoms observed in GSD-1a patients. This indicates that our model has great potential for clinical translation, and can provide insights into the relationship between residual hepatic G6PC activity, phenotype, and individualizing innovative treatments, such as

gene therapy and mRNA therapy. Whether this also applies to liver tumor development (e.g., the relationship between residual hepatic G6PC activity and liver tumor development<sup>(46-48)</sup>) requires further research. Moreover, functional restoration by gene therapy will typically also result in mosaic patterns of restored hepatic G6PC activity. Therefore, we expect that CRISPR/Cas9-mediated *G6pc* editing also provides a valuable tool to predict the outcome of G6PC gene therapy in patients exhibiting different degrees of residual G6PC activity. Finally, single-cell analysis of mosaic-patterned hepatocytes will potentially allow for the linking of specific genetic profiles to the tumorigenic potential of individual hepatocytes.

In conclusion, we show that CRISPR/Cas9-mediated gene editing of hepatic *G6pc* in mice opens perspectives for translational research on hepatic GSD-1a and other inherited liver diseases.<sup>(27,28,35,36)</sup> This powerful and versatile tool allows systematic and efficient investigation of the contribution of specific genes to (patho)physiology and compensatory mechanisms without extensive breeding schemes. A unique feature of this approach is that it enables one to assess the relationship between residual hepatic G6PC activity and heterogeneity in symptoms and complications (Supporting Table S7).<sup>(23-25)</sup> By generating a spectrum of disease symptoms in mice, the current work provides a step toward the evaluation of potential therapies in a patient-specific manner, hence ultimately contributing to personalized care for GSD-1a patients.

*Acknowledgment:* We thank S. de Neck, Y.T. van der Veen, J. van der Krogt, T.H. van Dijk, R. Havinga, F. Kuipers, I.A. Martini, M. Koehorst, V.W. Bloks, A. de Haan, A. Bleeker, J.A. Hoogerland, K.A. Krishnamurthy, M. Vos, A.J.C. Tol, and A.H. Heida for excellent technical assistance. We thank J. Chou (NIH) for providing us with the protocols for the microsomal preparations and phosphohydrolase assays and M.J. Lizak (NIH) for support with MRI procedures. We thank W.H. Lamers (Academic Medical Center) for providing us with the CK19 antibody.

*Author Contributions:* Designing research studies: M.G.S.R., T.G.J.D., B.S., and M.H.O., conducting experiments: M.G.S.R., N.C.A.H., T.B., N.J.K., C.W.A.K., J.C.W., M.H.K., analyzing data: M.G.S.R., T.B., C.W.A.K., J.C.W., L.B., R.E.T., A.B., B.S., and M.H.O., writing the first draft of the manuscript:

M.G.S.R., B.S. and M.H.O., critical revisions of the manuscript: C.W.A.K., R.E.T., A.B., T.G.J.D., B.S., and M.H.O.

## REFERENCES

- 1) Chou JY, Jun HS, Mansfield BC. Type I glycogen storage diseases: disorders of the glucose-6-phosphatase/glucose-6-phosphate transporter complexes. *J Inherit Metab Dis* 2015;38:511-519.
- 2) Bali DS, Chen YT, Austin S, Goldstein JL. Glycogen Storage Disease Type I. 2006 Apr 19 [Updated 2016 Aug 25]. In: Adam MP, Ardinger HH, Pagon RA, et al., eds. *GeneReviews*® [Internet]. Seattle, WA: University of Washington; 1993-2020. <https://www.ncbi.nlm.nih.gov/books/NBK1312/?report=classic>. Accessed July 11, 2021.
- 3) Rajas F, Clar J, Gautier-Stein A, Mithieux G. Lessons from new mouse models of glycogen storage disease type 1a in relation to the time course and organ specificity of the disease. *J Inherit Metab Dis* 2015;38:521-527.
- 4) Rake JP, Visser G, Labrune P, Leonard JV, Ullrich K, Smit GPA. Glycogen storage disease type I: diagnosis, management, clinical course and outcome. Results of the European Study on Glycogen Storage Disease Type I (ESGSD I). *Euro J Pediatr* 2002;161(Suppl. 1):S20-S34.
- 5) Visser G, Rake JP, Labrune P, Leonard JV, Moses S, Ullrich K, et al. Consensus guidelines for management of glycogen storage disease type 1b - European study on glycogen storage disease type 1. *Eur J Pediatr* 2002;161(Suppl. 1):S120-S123.
- 6) Kishnani PS, Austin SL, Abdenur JE, Arn P, Bali DS, Boney A, et al. Diagnosis and management of glycogen storage disease type I: a practice guideline of the American College of Medical Genetics and Genomics. *Genet Med* 2014;16:1-29.
- 7) Wang DQ, Fiske LM, Carreras CT, Weinstein DA. Natural history of hepatocellular adenoma formation in glycogen storage disease type I. *J Pediatr* 2011;159:442-446.
- 8) Beegle RD, Brown LM, Weinstein DA. Regression of hepatocellular adenomas with strict dietary therapy in patients with glycogen storage disease type I. *JIMD Rep* 2015;18:23-32.
- 9) Damska M, Labrador EB, Kuo CL, Weinstein DA. Prevention of complications in glycogen storage disease type Ia with optimization of metabolic control. *Pediatr Diabetes* 2017;18:327-331.
- 10) Okechuku GO, Shoemaker LR, Damska M, Brown LM, Mathew J, Weinstein DA. Tight metabolic control plus ACE inhibitor therapy improves GSD I nephropathy. *J Inherit Metab Dis* 2017;40:703-708.
- 11) Peeks F, Steunenberg TAH, de Boer F, Rubio-Gozalbo ME, Williams M, Burghard R, et al. Clinical and biochemical heterogeneity between patients with glycogen storage disease type IA: the added value of CUSUM for metabolic control. *J Inherit Metab Dis* 2017;40:695-702.
- 12) Peeks F, Boonstra WF, de Baere L, Carøe C, Casswall T, Cohen D, et al. Research priorities for liver glycogen storage disease: an international priority setting partnership with the James Lind Alliance. *J Inherit Metab Dis* 2020;43:279-289.
- 13) Lei Y, Hoogerland JA, Bloks VW, Bos T, Bleeker A, Wolters H, et al. Hepatic ChREBP activation limits NAFLD development in a mouse model for glycogen storage disease type Ia. *HEPATOLOGY* 2020;72:1638-1653.
- 14) Cho JH, Kim GY, Pan CJ, Anduaga J, Choi EJ, Mansfield BC, et al. Downregulation of SIRT1 signaling underlies hepatic autophagy impairment in glycogen storage disease type Ia. *PLoS Genet* 2017 13:e1006819.
- 15) Gjorgjieva M, Calderaro J, Monteillet L, Silva M, Raffin M, Brevet M, et al. Dietary exacerbation of metabolic stress leads to accelerated hepatic carcinogenesis in glycogen storage disease type Ia. *J Hepatol* 2018;69:1074-1087.
- 16) Cho JH, Kim GY, Mansfield BC, Chou JY. Sirtuin signaling controls mitochondrial function in glycogen storage disease type Ia. *J Inherit Metab Dis* 2018;41:997-1006.
- 17) Cho JH, Kim GY, Mansfield BC, Chou JY. Hepatic glucose-6-phosphatase- $\alpha$  deficiency leads to metabolic reprogramming in glycogen storage disease type Ia. *Biochem Biophys Res Commun* 2018;498:925-931.
- 18) Farah BL, Landau DJ, Sinha RA, Brooks ED, Wu Y, Fung SYS, et al. Induction of autophagy improves hepatic lipid metabolism in glucose-6-phosphatase deficiency. *J Hepatol* 2016;64:370-379.
- 19) Farah BL, Sinha RA, Wu Y, Singh BK, Lim A, Hirayama M, et al. Hepatic mitochondrial dysfunction is a feature of Glycogen Storage Disease Type Ia (GSDIa). *Sci Rep* 2017;7:44408.
- 20) Cangelosi D, Resaz R, Petretto A, Segalerba D, Ognibene M, Raggi F, et al. A proteomic analysis of GSD-1a in mouse livers: evidence for metabolic reprogramming, inflammation, and macrophage polarization. *J Proteome Res* 2019;18:2965-2978.
- 21) Monteillet L, Gjorgjieva M, Silva M, Verzieux V, Imikirene L, Duchamp A, et al. Intracellular lipids are an independent cause of liver injury and chronic kidney disease in non alcoholic fatty liver disease-like context. *Mol Metab* 2018;16:100-115.
- 22) Hijmans BS, Boss A, van Dijk TH, Soty M, Wolters H, Mutel E, et al. Hepatocytes contribute to residual glucose production in a mouse model for glycogen storage disease type Ia. *HEPATOLOGY* 2017;66:2042-2054.
- 23) Lei KJ, Chen H, Pan CJ, Ward JM, Mosinger B, Lee EJ, et al. Glucose-6-phosphatase dependent substrate transport in the glycogen storage disease type-1a mouse. *Nat Genet* 1996;13:203-209.
- 24) Mutel E, Abdul-Wahed A, Ramamonjisoa N, Stefanutti A, Houberton I, Cavassila S, et al. Targeted deletion of liver glucose-6-phosphatase mimics glycogen storage disease type 1a including development of multiple adenomas. *J Hepatol* 2011;54:529-537.
- 25) Resaz R, Vanni C, Segalerba D, Sementa AR, Mastracci L, Grillo F, et al. Development of hepatocellular adenomas and carcinomas in mice with liver-specific G6Pase- $\alpha$  deficiency. *DMM Dis Model Mech* 2014;7:1083-1091.
- 26) Chou JY, Mansfield BC. Mutations in the glucose-6-phosphatase- $\alpha$  (G6PC) gene that cause type Ia glycogen storage disease. *Hum Mutat* 2008;29:921-930.
- 27) Fedoseienko A, Wijers M, Wolters JC, Dekker D, Smit M, Huijkman N, et al. The COMMD family regulates plasma LDL levels and attenuates atherosclerosis through stabilizing the CCC complex in endosomal LDLR trafficking. *Circ Res* 2018;122:1648-1660.
- 28) de Boer JF, Verkade E, Mulder NL, de Vries HD, Huijkman N, Koehorst M, et al. A human-like bile acid pool induced by deletion of hepatic Cyp2c70 modulates effects of FXR activation in mice. *J Lipid Res* 2020;61:291-305.
- 29) Kishnani PS, Bao Y, Wu JY, Brix AE, Lin JL, Chen YT. Isolation and nucleotide sequence of canine glucose-6-phosphatase mRNA: Identification of mutation in puppies with glycogen storage disease type Ia. *Biochem Mol Med* 1997;61:168-177.
- 30) Kim GY, Lee YM, Cho JH, Pan CJ, Jun HS, Springer DA, et al. Mice expressing reduced levels of hepatic glucose-6-phosphatase-a activity do not develop age-related insulin resistance or obesity. *Hum Mol Genet* 2015;24:5115-5125.
- 31) Lee YM, Jun HS, Pan CJ, Lin SR, Wilson LH, Mansfield BC, et al. Prevention of hepatocellular adenoma and correction of metabolic abnormalities in murine glycogen storage disease type Ia by gene therapy. *HEPATOLOGY* 2012;56:1719-1729.



- 32) **Lee YM, Kim GY**, Pan CJ, Mansfield BC, Chou JY. Minimal hepatic glucose-6-phosphatase- $\alpha$  activity required to sustain survival and prevent hepatocellular adenoma formation in murine glycogen storage disease type Ia. *Mol Genet Metab Rep* 2015;3:28-32.
- 33) Clar J, Mutel E, Gri B, Creneugy A, Stefanutti A, Gaillard S, et al. Hepatic lentiviral gene transfer prevents the long-term onset of hepatic tumours of glycogen storage disease type Ia in mice. *Hum Mol Genet* 2015;24:2287-2296.
- 34) Hoogerland JA, Peeks F, Hijmans BS, Wolters JC, Kooijman S, Bos T, et al. Impaired very-low-density lipoprotein catabolism links hypoglycemia to hypertriglyceridemia in glycogen storage disease type Ia. *J Inherit Metab Dis* [Internet]. 2021; [cited 2021 May 14]. Available from: <https://pubmed.ncbi.nlm.nih.gov/33739445/>. <https://doi.org/10.1002/jimd.12380>. [Epub ahead of print]
- 35) Jarrett KE, Lee CM, Yeh YH, Hsu RH, Gupta R, Zhang M, et al. Somatic genome editing with CRISPR/Cas9 generates and corrects a metabolic disease. *Sci Rep* 2017;7:44624.
- 36) **Xue W, Chen S, Yin H**, Tammela T, Papagiannakopoulos T, Joshi NS, et al. CRISPR-mediated direct mutation of cancer genes in the mouse liver. *Nature* 2014;514:380-384.
- 37) Penhoat A, Fayard L, Stefanutti A, Mithieux G, Rajas F. Intestinal gluconeogenesis is crucial to maintain a physiological fasting glycemia in the absence of hepatic glucose production in mice. *Metabolism* 2014;63:104-111.
- 38) Mutel E, Gautier-Stein A, Abdul-Wahed A, Amigo-Correig M, Zitoun C, Stefanutti A, et al. Control of blood glucose in the absence of hepatic glucose production during prolonged fasting in mice: induction of renal and intestinal gluconeogenesis by glucagon. *Diabetes* 2011;60:3121-3131.
- 39) Krupke DM, Begley DA, Sundberg JP, Bult CJ, Eppig JT. The mouse tumor biology database. *Nat Rev Cancer* 2008;8:459-465.
- 40) Turturro A, Duffy P, Hass B, Kodell R, Hart R. Survival characteristics and age-adjusted disease incidences in C57BL/6 mice fed a commonly used cereal-based diet modulated by dietary restriction. *J Gerontol Ser A Biol Sci Med Sci* 2002;57:B379-B389.
- 41) Nakamura K, Kuramoto K, Shibasaki K, Shumiya S, Ohtsubo K. Age-related incidence of spontaneous tumors in SPF C57BL/6 and BDF1 mice. *Jikken Dobutsu* 1992;41:279-285.
- 42) Muruve DA, Barnes MJ, Stillman IE, Libermann TA. Adenoviral gene therapy leads to rapid induction of multiple chemokines and acute neutrophil-dependent hepatic injury in vivo. *Hum Gene Ther* 1999;10:965-976.
- 43) Lieber A, He CY, Meuse L, Schowalter D, Kirillova I, Winther B, et al. The role of Kupffer cell activation and viral gene expression in early liver toxicity after infusion of recombinant adenovirus vectors. *J Virol* 1997;71:8798-8807.
- 44) Suda T, Kamimura K, Kubota T, Tamura Y, Igarashi M, Kawai H, et al. Progress toward liver-based gene therapy. *Hepatol Res* 2009;39:325-340.
- 45) **Ran FA, Hsu PD**, Wright J, Agarwala V, Scott DA, Zhang F. Genome engineering using the CRISPR-Cas9 system. *Nat Protoc* 2013;8:2281-2308.
- 46) Kim GY, Lee YM, Kwon JH, Cho JH, Pan CJ, Starost MF, et al. Glycogen storage disease type Ia mice with less than 2% of normal hepatic glucose-6-phosphatase- $\alpha$  activity restored are at risk of developing hepatic tumors. *Mol Genet Metab* 2017;120:229-234.
- 47) Brooks ED, Landau DJ, Everitt JI, Brown TT, Grady KM, Waskowicz L, et al. Long-term complications of glycogen storage disease type Ia in the canine model treated with gene replacement therapy. *J Inherit Metab Dis* 2018;41:965-976.
- 48) Lee YM, Conlon TJ, Specht A, Coleman KE, Brown LM, Estrella AM, et al. Long-term safety and efficacy of AAV gene therapy in the canine model of glycogen storage disease type Ia. *J Inherit Metab Dis* 2018;41:977-984.

Author names in bold designate shared co-first authorship.

## Supporting Information

Additional Supporting Information may be found at [onlinelibrary.wiley.com/doi/10.1002/hep.32022/supinfo](https://onlinelibrary.wiley.com/doi/10.1002/hep.32022/supinfo).